Joule

Ex situ bismuth doping for efficient CdSeTe thin-film solar cells with open-circuit voltages exceeding 900 mV

Graphical abstract

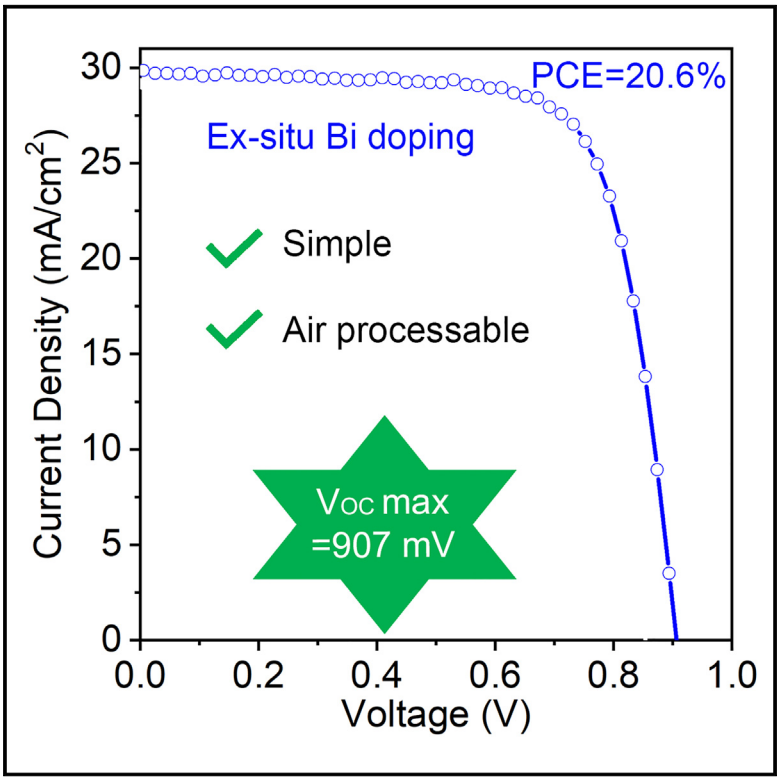

Authors

Sabin Neupane, Deng-Bing Li, Abasi Abudulimu, ..., William Huber, Gang Xiong, Yanfa Yan

Correspondence

dengbing.li@utoledo.edu (D.-B.L.), yanfa.yan@utoledo.edu (Y.Y.)

In brief

Ex situ Bi-doped CdSeTe thin-film solar cells achieve a champion power conversion efficiency of 20.6% and open-circuit voltages over 900 mV. *Ex situ* Bi doping is simple and can be processed in the air.

Highlights

- *Ex situ* Bi-doped CdSeTe solar cells reached power conversion efficiencies of up to 20.6%
- *Ex situ* Bi-doped CdSeTe solar cells demonstrated V_{OC}s exceeding the 900 mV mark
- The Se-rich region promotes Bi ions to occupy the anion site
- *Ex situ* Bi doping can be processed in the air

Neupane et al., 2025, Joule 9, 101766
January 15, 2025
https://doi.org/10.1016/j.joule.2024.09.013

CellPress

Joule

CellPress

Article

Ex situ bismuth doping for efficient CdSeTe thin-film solar cells with open-circuit voltages exceeding 900 mV

Sabin Neupane,[1] Deng-Bing Li,[1,*] Abasi Abudulimu,[1] Manoj Kumar Jamarkattel,[1] Chun-Sheng Jiang,[2] Yeming Xian,[1] Xiaomeng Duan,[3] Adam B. Phillips,[1] Michael J. Heben,[1] Randall J. Ellingson,[1] Feng Yan,[3] Dingyuan Lu,[4] Dan Mao,[5] Nicholas Miller,[5] James Becker,[5] William Huber,[5] Gang Xiong,[4] and Yanfa Yan[1,6,*]

[1]Wright Center for Photovoltaic Innovation and Commercialization, Department of Physics and Astronomy, University of Toledo, Toledo, OH, USA

[2]National Renewable Energy Laboratory, Golden, CO, USA

[3]School for Engineering of Matter, Transport and Energy, Arizona State University, Tempe, AZ, USA

[4]California Technology Center, First Solar Inc., Santa Clara, CA, USA

[5]First Solar Inc., Perrysburg, OH, USA

[6]Lead contact

*Correspondence: dengbing.li@utoledo.edu (D.-B.L.), yanfa.yan@utoledo.edu (Y.Y.)

https://doi.org/10.1016/j.joule.2024.09.013

CONTEXT & SCALE Doping with group V elements has become widely recognized as a key strategy for enhancing power conversion efficiency and operational stability of CdSeTe solar cells. *In situ* group-V-doped CdSeTe solar cells have achieved a record power conversion efficiency of 23.1%. In this study, we introduce an *ex situ* bismuth (Bi)-doping method to fabricate efficient CdSeTe solar cells. This doping technique is straightforward and highly resilient to air processing conditions. The best-performing *ex situ* Bi-doped CdSeTe solar cell reached a power conversion efficiency of 20.6%. Notably, the cells also exhibited open-circuit voltages surpassing the 900 mV threshold, which was previously attained by *in situ* group V doping.

SUMMARY

The focus of CdSeTe thin-film solar cell doping has transitioned from copper (Cu) doping to group V doping. *In situ* group V doping has resulted in a new record power conversion efficiency (PCE) of 23.1%, with open-circuit voltages (V_{OC}s) exceeding the 900 mV mark. Here, we report that *ex situ* bismuth (Bi)-doped CdSeTe thin-film solar cells show V_{OC}s exceeding 900 mV and a champion PCE of 20.6%. Characterizations revealed that the Se-rich CdSeTe region near the front junction promotes Bi ions to occupy the anion sites and dope this region weakly p-type. Bi ions in the CdTe-dominating back surface region occupy the cation sites and are oxidized. This *ex situ* Bi doping with BiF_3 as a dopant precursor offers several advantages, including simplicity, high tolerance to the processing environment, and no requirement of additional Cd vapor or special activation processes, making it highly adaptable for researchers to explore efficient Bi-doped CdSeTe thin-film solar cells.

INTRODUCTION

CdSeTe thin-film solar cells are a highly competitive photovoltaic (PV) technology due to their low cost, high stability, and short energy payback time. As of 2023, more than 50 GW of CdTe solar modules have been installed worldwide, and the fabrication capacity is predicted to increase to 25 GW by 2026 from the current 9 GW.[1–3] Notably, CdSeTe thin-film PV has demonstrated a new record power conversion efficiency (PCE) of 23.1% for small cells and 19.7% for modules.[4,5] Despite this remarkable progress, CdSeTe thin-film PV still has considerable room for further PCE improvement that could further reduce its levelized cost of energy. Among all PV parameters, reducing open-circuit voltage (V_{OC}) deficit and improving long-term stability are the two most critical topics in CdSeTe thin-film PV research.[6–8]

In recent years, the CdSeTe thin-film PV research community has reached a consensus that shifting the dopant from the traditional copper (Cu) to group V elements is a viable strategy to reduce the V_{OC} deficit and improve stability.[9–14] Group V dopants are expected to have less self-doping compensations and lower diffusion coefficients than Cu dopants.[14,15] While the less self-doping compensations can help increase the hole

density, reducing the V_{OC} deficit, the lower diffusion coefficients should improve the device stability. Previous studies on group-V-doped CdTe single crystals have demonstrated a 100-fold increase in hole density and cells with V_{OC} exceeding 1 V.[9] Danielson et al. demonstrated a hole density of $7 \times 10^{16}/cm^3$ through *in situ* arsenic (As) doping combined with an additional $CdCl_2$ treatment.[10] Other studies have also shown much-improved p-type conductivity and device stability using group V doping.[11–14] However, for a long time, the substantial absorber quality improvement through group V doping did not translate into expected V_{OC} and PCE improvements as compared with Cu doping.[16–22] It was only that recently First Solar, the leading CdSeTe solar panel manufacturer, reported a PCE of 22.3% with a V_{OC} exceeding the 900 mV mark through *in situ* As doping.[23]

So far, most reported efficient group-V-doped CdSeTe solar cells are based on *in situ* As doping.[21–25] It has been reported that *in situ* As doping requires carefully controlled processes and special dopant activation, such as steps to crack As clusters, avoiding oxidation, and providing excessive Cd vapor, etc., to achieve high V_{OC}s and PCEs.[9,14,26] Advanced equipment, such as specially designed vapor transport deposition system and As cracking supplier, is often needed to meet these requirements, prohibiting many research groups from fabricating efficient and stable CdSeTe thin-film solar cells using *in situ* As doping. We recently developed an *ex situ* doping method to incorporate group V dopants in CdSeTe solar cells. By using $AsCl_3$ as a dopant source, we successfully fabricated CdSeTe thin-film solar cells with 18% PCE and 863 mV V_{OC}.[11] This strategy introduced a desired gradient dopant profile, i.e., a higher concentration in the back surface region and a lower concentration in the region near the front junction, helping reduce the front interfacial recombination velocity and revealing a potential method for further improvement of device performance. However, the use of $AsCl_3$ as a doping source faces several challenges. $AsCl_3$ is highly volatile (boiling point 130.2°C), oxygen sensitive, and toxic. As a result, the doping process must be conducted in an inert-gas-filled glovebox. Additionally, successful *ex situ* As doping using $AsCl_3$ source requires a porous carbon paste electrode to serve as a "reservoir" to prohibit the loss of $AsCl_3$ from the back surface. The high resistivity of the mesoporous carbon paste limits the fill factor (FF) of CdSeTe thin-film solar cells to below 72%. Therefore, implementing $AsCl_3$ as an As source still limits its widespread adoption by other research groups.

In this work, we report a strategy to overcome the abovementioned issues related to *ex situ* As doping. Instead of $AsCl_3$, we use more stable and less toxic BiF_3 as the dopant source for *ex situ* doping. One benefit of this approach is that the doping process can be conducted in ambient air and no inert gas protection is required, avoiding the need for a glovebox. Additionally, due to the less volatile and high ionic characteristics of BiF_3, the doping process does not require a resistive mesoporous carbon paste electrode to serve as the dopant reservoir, nor does it require excessive Cd vapor or additional high-temperature activation processes. The facile doping process significantly improved the reproducibility of efficient Bi-doped CdSeTe solar cell fabrication. Using CdSeTe film stacks provided by First Solar, our *ex situ* Bi-doped CdSeTe thin-film solar cells showed V_{OC}s exceeding the 900 mV mark and a champion PCE of 20.6% without the application of an anti-reflection coating. Our characterization and analysis revealed that despite a larger ionic size than the As ion, Bi ions can diffuse to the Se-rich CdSeTe region near the front junction and occupy the anion sites, doping this region weakly p-type. In the CdTe-dominating back surface region, Bi ions occupy the cation sites and are oxidized. The formation of Bi_2O_3 layer may reduce the quality of the back surface and limit the FF and PCE of the devices. This issue may be overcome in future studies by developing methods to better control the quantity and uniformity of the dopant source.

RESULTS AND DISCUSSION

For *ex situ* Bi doping, BiF_3 solution was prepared by dissolving 99.6% pure BiF_3 in HCl (14 wt %) to make a concentration of 6×10^4 mg/L. 150 μL BiF_3 solution was spin coated on top of a $CdCl_2$-treated CdSeTe surface at a spin speed of 7,000 rpm for 30 s. Then, the sample was annealed for 10 min at 310°C on a hot plate in air. The annealing temperature and duration significantly influence the final performance of Bi-doped devices (Figures S1 and S2). For devices with poly[bis(4-phenyl) (2,4,6-trimethylphenyl) amine] (PTAA), 20 mg/mL PTAA solution dissolved in toluene was spin coated on top of BiF_3-doped samples at a speed of 3,000 rpm for 20 s, followed by annealing on a hot plate at 150°C for 10 min. 50 nm gold (Au) back electrodes were deposited by thermal evaporation. The details of CdSeTe solar cell fabrication process at the University of Toledo were described elsewhere.[27,28]

Figure 1A and Table 1 show the current density-voltage (J-V) curves of the champion CdSeTe thin-film solar cells using *ex situ* Cu and Bi doping using the CdSeTe film stacks provided by First Solar Inc. CuSCN was used as a hole transfer material (HTM) and the Cu dopant source for the Cu-doped CdSeTe solar cells. The details of Cu doping are described in our earlier publications.[27–29] The champion Cu-doped device shows a PCE of 20.4% with a V_{OC} of 857 mV, whereas the Bi-doped champion device without an HTM shows a comparable PCE of 20.6% but with a higher V_{OC} of 874 mV. The undoped champion CdSeTe cell shows a PCE below 5%, with a V_{OC} lower than 500 mV. The significant V_{OC} improvement from 857 to 874 mV indicates improved front junction quality and demonstrates the effective doping effect of BiF_3. The external quantum efficiency (EQE) curves of these devices, shown in Figure 1B, reveal improved carrier collections in the short wavelength regions for the Bi-doped device, confirming a higher quality of both the front junction and the absorber region near this junction and yielding an integrated short-circuit current density (J_{SC}) of 29.97 mA/cm^2, within 5% variation of the J_{SC} obtained from the J-V measurement. It is noted that the champion Bi-doped device exhibits a higher V_{OC} but a slightly lower FF than the champion Cu-doped cell. The slightly reduced FF is due to the slightly larger series resistances (R_S) (3.51 Ω cm^2) in the Bi-doped device than those (1.9 Ω cm^2) in the Cu-doped device, with the underlying reason being discussed later. We fabricated 20 Cu-doped and 20 Bi-doped CdSeTe thin-film solar cells. The statistics of the performance of these cells are shown in Table S1 and Figure S3. The results

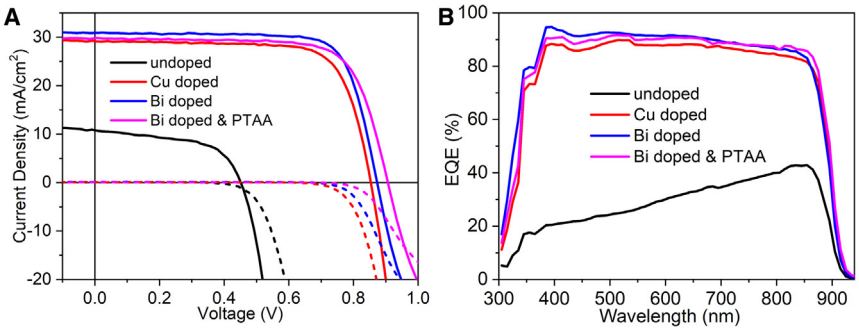

Figure 1. Device performance

(A) J–V curves of champion CdSeTe solar cells with *ex situ* Cu and Bi doping.

(B) EQE curves of champion CdSeTe solar cells with *ex situ* Cu and Bi doping. For comparison, the J-V and EQE curves of typical undoped samples and a representative Bi-doped solar cell with PTAA HTM are plotted.

clearly show that Bi doping yields higher V_{OC}s and smaller deviations than Cu doping. Whereas the Bi-doped cells demonstrated an average V_{OC} of 878 mV with a deviation of 5.5 mV, the Cu-doped devices presented a lower average V_{OC} of 858 mV with a higher deviation of 6.5 mV.

We have previously observed that using CuSCN as an HTM can improve the V_{OC} of our Cu-doped CdSeTe solar cells due to the passivation effect of HTMs on the back surface.[30] Therefore, we employed HTMs to further improve the V_{OC} of Bi-doped CdSeTe thin-film solar cells. To avoid the potential unintentional Cu doping from Cu-containing HTMs, several Cu-free organic HTMs, such as PTAA, Spiro-OMeTAD, and poly(3,4-ethylenedioxythiophene):poly(styrene sulfonate) (PEDOT:PSS), which are widely used in organic and hybrid perovskite solar cells, were applied in our Bi-doped devices. Our quick screening revealed that PTAA led to the best device performance. Therefore, only the results with PTAA are discussed in this paper. The statistical performance of 20 Bi-doped cells, with and without PTAA, is shown in Figure S4. As expected, employing PTAA as HTM led to additional improvements in V_{OC}. The average V_{OC} is further increased to 892 from 878 mV. It is noteworthy that 4 out of 20 measured cells showed $V_{OC} > 900$ mV, with a champion V_{OC} of 907 mV. However, due to the reduced FF, this V_{OC} improvement induced by employing a PTAA HTM did not translate into further improvement in PCE. The improvement in V_{OC} can be primarily attributed to the electron-blocking effect of PTAA, whereas the reduction of FF is likely caused by the PTAA layer, which has a poor electrical conductivity. Given the rough surface of CdSeTe films, a relatively thick PTAA layer (~50 nm, Figure S5) was employed to ensure full coverage of the CdSeTe surface. Mitigating the issues of conductivity and thickness conformity of the HTM layer may result in higher device performance.

To understand the origin of the improved PCE and V_{OC} of our Bi-doped CdSeTe thin-film solar cells, cross-sectional Kelvin probe force microscopy (KPFM) was conducted to examine the junction properties of the cells by imaging the electrical potential across the devices. The details of cross-sectional KPFM were described elsewhere.[31] Figures 2A and 2B show the cross-sectional potential images of an undoped and a Bi-doped CdSeTe solar cell, respectively, under a −1.5 V reverse bias applied to the devices, revealing the physical locations of the junctions. Figures 2C and 2D show the electric field difference profiles of the corresponding devices under different applied bias, −1.0 and −1.5 V, derived from the KPFM potential images and profiles under 0, −1.0, and −1.5 V bias (Figure S6). The undoped CdSeTe solar cell shows a very narrow electric field near the front junction, indicating the lack of efficient charge separation, accounting for the low PCE. The presence of an electric field near the back contact is likely attributed to the formation of a Schottky junction that indicates a potential barrier to hole extraction. Upon Bi doping, the electric field at the front junction extends into the CdSeTe absorber region, with an estimated depth of 2.4 μm. This electric field can help separate photogenerated electron and hole pairs, leading to reduced nonradiative recombination in this region and, therefore, much-improved device performance. The feature of this electric field is very similar to those observed in Cu-doped CdSeTe thin-film solar cells,[28,31,32] verifying that our *ex situ* doping creates a high-quality p-n junction near the front junction. Additionally, the Bi doping removes the electric field at the back contact, accounting for improved hole extraction. The KPFM results suggest that *ex situ* Bi doping increased the hole density in the CdSeTe absorber.

Scanning electron microscopy (SEM) analysis indicates that after Bi doping, the CdTe film surface reacted with the BiF_3 dopant source (Figures 3A and S7). As indicated by the arrow in Figure 3A, after Bi doping, small particles aggregate at grain boundary regions. X-ray energy dispersive spectroscopy (EDS) shows higher Bi concentration at grain boundary regions than grain surfaces (Figure S7). We anticipate that Bi ions diffuse preferentially through gain boundaries. Besides Bi, the EDS in Figure S7 also shows higher oxygen concentration at the grain boundary than in the grain interior, suggesting the formation of Bi_2O_3 at grain boundaries. We conducted time-of-flight secondary ion mass spectrometry (ToF-SIMS) measurement to examine the depth profile of Bi throughout the device. It is noted that the CdSeTe film stack used for the ToF-SIMS measurement was fabricated at the University of Toledo. It has a slightly different Se depth profile than the CdSeTe film fabricated at First Solar. A Bi-doped CdSeTe film was peeled off from the FTO substrate using the thermomechanical method. The ToF-SIMS measurement was conducted from the front junction side to avoid potential artificial effects induced by the rough back surface. As depicted in Figure 3B, the *ex situ* doping introduced a Bi concentration gradient, i.e., the Bi concentration near the back surface is 3–4 orders of magnitude higher than that in the middle region. The Bi concentration in the built-in region near the front junction is nearly below the ToF-SIMS detection limit, $\sim 2 \times 10^{17}/cm^3$. However, an accumulation of Bi near the front interface is clearly observed adjacent to the FTO substrate, suggesting grain-boundary-assisted Bi diffusion. We also conducted ToF-SIMS

Table 1. J-V parameters for the champion CdSeTe solar cells with *ex situ* Cu and Bi doping

Devices	V_{OC} (mV)	J_{SC} (mA/cm^2)	FF (%)	PCE (%)
Undoped	451	10.8	54.8	2.67
Cu-doped	857	30.3	78.3	20.4
Bi-doped	874	30.9	76.2	20.6
Bi-doped and PTAA	907	29.8	73.3	19.8

For comparison, a typical undoped cell and a representative Bi-doped solar cell with PTAA hole transport material are also included.

analysis to examine the Cu profiles in Bi-doped, Cu-doped, and undoped CdSeTe samples. We did not detect noticeable unintentional Cu contaminations in Bi-doped and undoped samples. The results confirm that the p-type doping effects in Bi-doped CdSeTe cells are not caused by unintentional Cu doping. X-ray photoelectron spectroscopy (XPS) mapping (Figure 3C) on a Bi-doped CdSeTe surface shows inhomogeneity of Bi distribution. The feature is very similar to that of the grain boundary distribution, confirming that Bi atoms diffused primarily through grain boundaries.

We performed depth-dependent XPS measurements to understand the doping mechanism. The spectrum of Bi 4f states obtained from the back surface (0 s of sputtering, Figure 3D) shows two sets of peaks with binding energies, of which 159.7 and 165.1 eV correspond to Bi-O bonding and 158.2 and 163.6 eV correspond to Bi-Te bonding. The high intensity of Bi-O bonding at the surface suggests that Bi atoms on the surface are partially oxidized due to the annealing in air, similar to the oxidization of Cd at the back surface (Figure S8A). Meanwhile, the presence of Bi-Te bonding reveals that some Bi atoms can occupy Cd site. When the surface was sputtered by Ar ions for 300 s, the Bi-Te bonding peaks became more pronounced. This suggests that more Bi atoms occupy Cd sites rather than being oxidized in the region below the surface. Meanwhile, another peak appeared with a binding energy of 169.4 eV when the film was milled deeper from the back surface, which can be assigned to the Cd-Bi bonding. As the sputtering time increased, the intensities of the peaks associated with Bi-Te bonding decreased but the intensity of the peak associated Cd-Bi bonding did not. Therefore, as the depth increased from the film surface, the density of Bi atoms on Cd sites decreased, and the density of Bi atoms on Te sites increased, which is consistent with the gradient profile of Se. We also peeled off a Bi-doped CdSeTe film and conducted depth-dependent XPS measurements from the front side (Figure 3E). The XPS spectra showed three peaks, with binding energies of 159.1, 164.5, and 167.2 eV corresponding to Bi-Se (first two peaks) and Cd-Bi bonding, respectively. We noted that the Cd-Bi bonding energy gradually increased from 167.2 eV at the front surface to 167.8 eV as the depth increased after etching for 20 min. This change can be attributed to the gradient change of S, Se, and Te in the absorber, which can be demonstrated from the binding energy shift of Cd at the front interface (Figure S8C). After Ar ion sputtering for 20 min, these peaks remained, confirming that upon annealing Bi atoms diffuse into the front junction through grain boundaries. The Bi-related XPS data with depth are consistent with those obtained from ToF-SIMS. However, the XPS results revealed that Bi atoms can occupy both Cd and Te sites. Density functional theory calculations (Figure S9) demonstrated that a shallow donor is formed when Bi is at a Cd site, whereas an acceptor is formed when Bi occupies a Te site. The net conductivity and carrier density depend on the ratio of these occupancies. Currently, there is no technique available to measure the ratio accurately. Therefore, we measured the net hole density profiles of the *ex situ* Bi-doped CdSeTe thin-film solar cell via capacitance-voltage (C-V) measurement. As shown in Figure 3F, the hole density in the Bi-doped device is about 1.75×10^{14}/cm^3 at the minimum point of the C-V curve, which is slightly lower than that of the Cu-doped device (5.27×10^{14}/cm^3) and *ex situ* As-doped device (2.51×10^{15}/cm^3). Based on the Bi concentration of about 2×10^{17}/cm^3 obtained from ToF-SIMS measurement, the Bi activation ratio is calculated to be lower than 0.09%. Such a low activation ratio is consistent with Bi aggregation at the front interface and grain boundaries. To further improve the activation ratio, further optimization of the annealing conditions and improvement on the CdTe film quality with larger grain sizes that can reduce Bi aggregation at the front interface and grain boundaries are needed. Furthermore, supplying Cd vapor during the doping process may also help increase the activation ratio.

Steady-state photoluminescence (PL) and time-resolved PL (TRPL) measurements confirm that *ex situ* Bi doping reduces the nonradiative recombination in the absorber region near the front junction. Figure 4A shows two PL spectra measured from the glass sides of undoped and Bi-doped CdSeTe samples. It is seen that after Bi doping, the PL intensity increased by more than three times, even higher than the PL spectra measured from Cu-doped samples. The increased PL intensity indicates the reduced density of nonradiative centers in the front region. The TRPL curve (Figure 4B), measured from the glass side of a Bi-doped CdSeTe film, shows a Tau_1 lifetime of 219 ns and a Tau_2 lifetime of 801 ns, which are longer than those in the undoped (68 and 281 ns, respectively) and Cu-doped CdSeTe film (157 and 645 ns, respectively). The TRPL results confirm that Bi doping improves the quality in the front junction region. We also measured TRPL curves from the film side of undoped and Bi-doped CdSeTe films but could not measure any meaningful lifetime due to the high nonradiative recombination caused by the back surface. For Bi-doped films, the high dopant density and remnant Bi_2O_3 are expected to create a high density of defects, leading to low quality of the back surface, which is responsible for the relatively low FF of Bi-doped devices. This is consistent with our J-V-T measurements of *ex situ* Cu- and Bi-doped CdSeTe solar cells (Figures 4C and S10). Whereas the measured back barrier height is 0.384 ±0.018 eV for the Bi-doped cell, it is 0.318 ± 0.010 eV for a Cu-doped cell. In our doping process, the BiF_3 dopant source was applied by solution process. However, this process does not provide an accurate control of the amount and the uniformity of BiF_3. Further development of the process with improved control of the dopant source would help improve the quality of the back surface, which will further improve the V_{OC} and FF of *ex situ* Bi-doped CdSeTe thin-film solar cells.

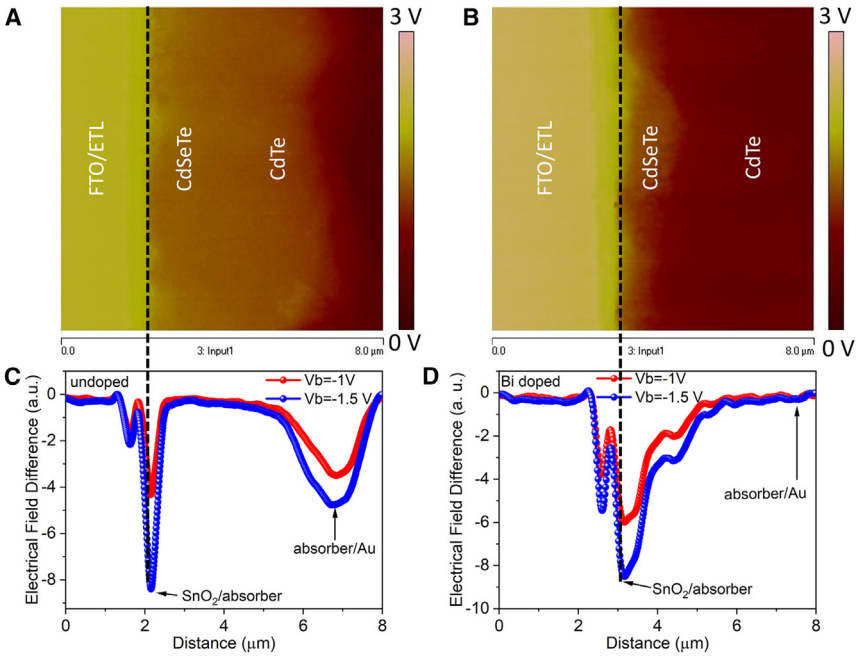

Figure 2. Heterojunction characterization

(A) Cross-sectional Kelvin probe force microscopy (KPFM) images from undoped CdSeTe thin-film solar cells.

(B) Cross-sectional Kelvin probe force microscopy (KPFM) images from Bi-doped CdSeTe thin-film solar cells.

(C) Electric field difference profiles under different bias (−1 and −1.5 V) from undoped CdSeTe thin-film solar cells.

(D) Electric field difference profiles under different bias (−1 and −1.5 V) from *ex situ* Bi-doped CdSeTe thin-film solar cells.

The 99.6% purity BiF_3 source used in this study contains a higher concentration of Ag than Cu. To exclude the impact of unintentional Ag doping, we fabricated CdSeTe thin-film solar cells using a 99.99% pure BiF_3 source. The Ag concentration in the high-purity BiF_3 source is three orders of magnitude lower than that in the 99.6% pure BiF_3. The annealing process was modified to rapidly ramp up the temperature to 320°C, then slowly cool it down to room temperature, to optimize the device performance. As shown in Figure S11, the V_{OC}s of *ex situ* Bi-doped CdSeTe cells using this high-purity BiF_3 source can also reach the 900-mV mark. We also purposely added various amounts (0.00025, 0.00040, 0.00050, and 0.00057 wt %) of AgSCN in the 99.99% high-purity BiF_3 source to evaluate the impact of unintentional Ag doping. As shown in Figure S12, adding Ag led to lower V_{OC}s and PCEs. We have also fabricated Ag-doped CdSeTe solar cells using AgSCN as the doping source and HTM. Both Cu-doped and Ag-doped CdSeTe solar cells showed lower V_{OC}s and PCEs than Bi-doped cells. Our results confirm that the high V_{OC}s and PCEs of *ex situ* Bi-doped CdSeTe solar cells cannot be attributed to unintentional Cu or Ag doping.

Conclusions

In conclusion, we have demonstrated CdSeTe thin-films solar cells achieving a champion PCE of 20.6% and V_{OC}s exceeding the 900-mV mark using *ex situ* Bi doping with BiF_3 as a dopant source. The self-compensation of Bi dopants at cation and anion sites limited the net hole density, but it did not limit the V_{OC} of the device. Oxidation of Bi atoms at the back surface was identified as a limiting factor for the FF of the devices. Therefore, precise control of the amount and uniformity of the applied dopant source is necessary to enhance the performance of *ex situ* Bi-doped CdSeTe solar cells. The facile process of *ex situ* group V doping by utilizing BiF_3 as a dopant source opens an opportunity for the CdSeTe solar cell community to explore efficient and stable Bi-doped CdSeTe solar cells.

EXPERIMENTAL PROCEDURES

Materials

The 99.6% purity BiF_3 powders were purchased from Alfa Aesar and the 99.99% purity BiF_3 powders were purchased from Sigma Aldrich. HCl was purchased from Fisher Chemical, HNO_3 was purchased from VWR Chemicals, and Li-TFSI was purchased from Thermo Fisher. PTAA, tBP solution, toulene, and acetonitrile were purchased from Sigma-Aldrich.

Device fabrication

In this work, two kinds of CdTe stack were used for device fabrication and the subsequent characterizations. One is the $CdCl_2$-treated CdSeTe stacks supplied by First Solar Inc., which were used for the optimization of Bi doping as well as the PL, capacitance-voltage, temperature-dependent J-V characterizations. Other than that, CdSSeTe devices fabricated in University of Toledo were applied using our reported method.[27,28] BiF_3 solution was prepared by dissolving the BiF_3 powder in HCl (14 wt %). PTAA solution was prepared by dissolving 20 mg PTAA in 1 mL toluene, followed by adding 15 µL Li-TFSi (170 mg/mL in acetonitrile) and 10 µL tBP solution. Then, the BiF_3 solution was spin coated on $CdCl_2$-treated stacks at 7,000 rpm, followed by heat treatment at 310°C for 10 min on a hotplate in ambient air. After that, the sample was spin coated with 50 µL PTAA solution followed by 10 min heat treatment at 150°C on a hotplate in ambient air. Finally, 50 nm gold (Au) was evaporated as electrode with 0.08 cm^2 shadow mask. The Cu doping for our reference devices was conducted using our reported procedure.[28,29]

Device characterization

The solar cell performance was characterized at room temperature in air by measuring current density-voltage (J-V) curves, with a scanning speed of 200 mV/s under AM1.5G illumination using a solar simulator (PV Measurements Inc.) and a source meter (Keithley 2400). The light intensity for the J-V measurements was calibrated by a standard silicon wafer solar cell certified by Newport. Before J-V measurement, light soaking treatment was carried out for all the devices at 85°C under AM1.5G illumination for 15 min. A quantum efficiency system (model IVQE8-C, PV Measurements Inc.) was used to measure the quantum efficiency of the PSCs. A standard silicon wafer solar cell was used as the reference for the EQE measurement. KPFM measurements were performed on a home-built KPFM system based on a Vecco D3100 atomic force microscope. A PPP-EFM (nanosensors) tip was operated in tapping mode for the cross-sectional potential distribution using second harmonic oscillation of the cantilever. The electrical resolution was ~10 mV. In the junction measurement, we cleaved and carefully ion milled the solar cell to expose the cross-sectional surface, following the conditions mentioned in Jiang et al.[31] and Moutinho et al.[32] the FTO was grounded, and various bias

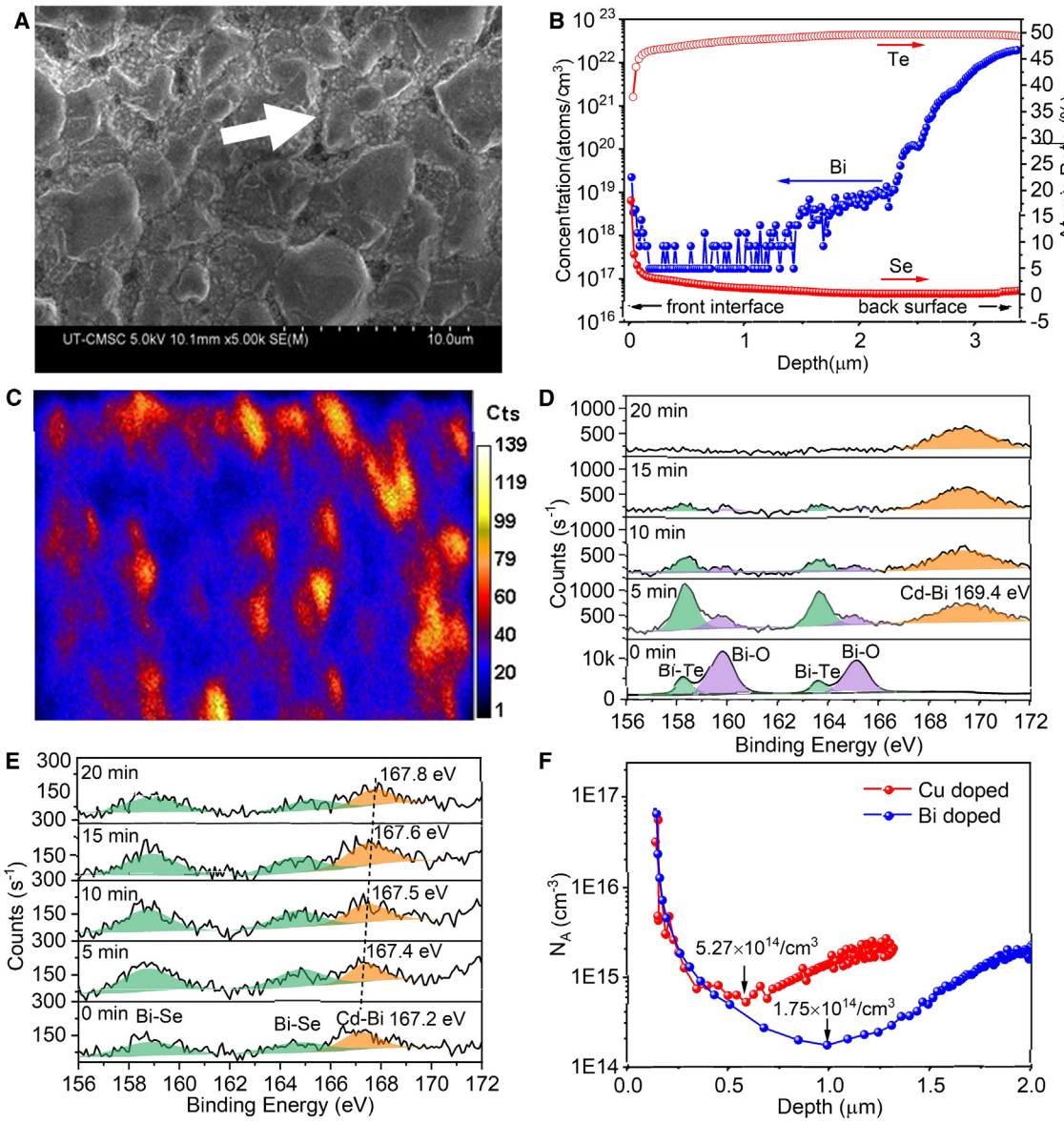

Figure 3. Distribution of Bi in CdSeTe films

(A) SEM image of the back surface of a Bi-doped CdSeTe sample.

(B) ToF-SIMS depth profiles for a Bi-doped CdSeTe device.

(C) XPS Bi mapping of the surface of a Bi-doped CdSeTe film.

(D) Depth-dependent XPS spectra measured from the back surface.

(E) Depth-dependent XPS spectra measured from the front surface.

(F) Hole density profiles obtained from the capacitance-voltage (C-V) measurements in Cu-doped and Bi-doped CdSeTe devices. The hole density values were obtained at the lowest point of the curves.

voltages (0, −1, and −1.5 V) were applied to the Au side. Surface imaging and X-ray EDS measurements were performed using a Hitachi-4800S SEM. The ToF-SIMS analyses were performed on a Cameca IMF-6f (810 Kifer Road, Sunnyvale, CA) double-focusing magnetic sector instrument. The samples were bombarded by a focused Cs^+ primary ion beam with a net impact energy of 5 keV and about 100 nA of beam current. The beam is rastered over a square area of 200 μm on a side. The secondary ions formed from the sputtering process are accelerated away from the sample surface by a nominal sample voltage of 5 kV. A fraction of secondary ions are collected from a circular region centered in the rastered area. The steady-state PL spectra were measured in a custom-built system, equipped with Horiba Symphony-II CCD detector and Horiba iHR320 monochromator, exciting the samples with 633 nm continuous wave lasers (2.5×10^{17} cm^{-2} S^{-1}). The time-resolved PL measurements were done with a Becker & Hickl TCSPC (HPM100-50, SPM130)-based system equipped with Fianium supercontinuum laser exciting the sample at 633 nm (1,011 cm^{-2} $pulse^{-1}$). High-resolution XPS was measured with a monochromatic aluminum X-ray source (model 5600, PerkinElmer). The C-V measurements were performed in the dark with

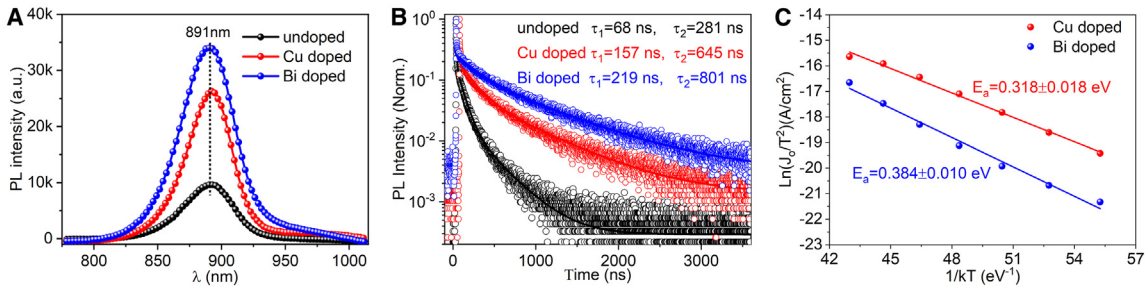

Figure 4. Carrier lifetime and back-barrier height

(A) PL spectrum measured from the glass side of undoped, Cu-doped, and Bi-doped CdSeTe thin films using a 632 nm excitation laser.

(B) TRPL curves measured from the glass side of undoped, Cu-doped, and Bi-doped CdSeTe thin films using a 632 nm excitation laser.

(C) The back barrier heights of Cu- and Bi-doped CdSeTe solar cells derived from J-V-T curves of Cu- and Bi-doped CdSeTe solar cells.

a constant 45-mV r.m.s. 10 kHz AC signal superimposed on a DC bias voltage varying from 2.5 to 0.5 V.

DFT calculation

The Bi_{Cd} and Bi_{Te} point defects were obtained by manual structural modification in a 2 × 2 × 2 cubic CdTe supercell with lattice constant of 13.27 Å that contains 32 Cd atoms and 32 Te atoms, followed by atomic position relaxation. The self-consistent partial density of states (PDOSs) calculations of the defective configurations were performed with the Vienna Ab-initio Simulation Package (VASP) code at the HSE06 + SOC level, where the fraction of exact exchange was set to 0.37, yielding a calculated band gap of pristine CdTe supercell of 1.44 eV.[33–36] The wavefunctions were expanded by adopting an energy cutoff value of 300 eV. A 3 × 3 × 3 k-point mesh grid was employed to sample the Brillouin zone.[37]

RESOURCE AVAILABILITY

Lead contact

Further information and requests for resources should be directed to and will be fulfilled by the lead contact, Yanfa Yan (yanfa.yan@utoledo.edu).

Materials availability

This study did not generate new unique reagents.

Data and code availability

All data are present in the paper and supplemental information. Other data are available from the lead contact or corresponding author.

ACKNOWLEDGMENTS

This work is based on research sponsored by Air Force Research Laboratory under agreement numbers FA9453-18-2-0037 and FA9453-21-C-0056, National Science Foundation (contract numbers 1665028, 1711534, and 1944374), and the US DOE's Office of Energy Efficiency and Renewable Energy (EERE) under Solar Energy Technologies Office (SETO) agreement DE-EE0008974, Cadmium Telluride Accelerator Consortium (CTAC) (NREL sub-contract SUB-2021-10715). The views expressed are those of the authors and do not reflect the official guidance or position of the United States Government, the Department of Defense, or of the United States Air Force. The appearance of external hyperlinks does not constitute endorsement by the United States Department of Defense (DoD) of the linked websites or the information, products, or services contained therein. The DoD does not exercise any editorial, security, or other control over the information you may find at these locations. DFT calculations used resources of the National Energy Research Scientific Computing Center, a DOE Office of Science User Facility supported by the Office of Science of the US Department of Energy under contract number DE-AC02-05CH11231 using NERSC award BES-ERCAP0023945.

AUTHOR CONTRIBUTIONS

Conceptualization, D.-B.L., S.N., and Y.Y.; methodology, S.N. and D.-B.L.; investigation, S.N., D.-B.L., D.L., and D.M.; writing – original draft, S.N., D.-B.L., and Y.Y.; validation, A.A., M.K.J., C.-S.J., D.L., D.M., J.B., N.M., F.Y., and X.D.; software calculation, Y.X.; writing – review & editing, D.-B.L., F.Y., M.J.H., and Y.Y.; funding acquisition, M.J.H., R.J.E., and Y.Y.; resources, A.P., D.L., J.B., W.H., G.X., J.B., and Y.Y.; supervision, Y.Y.

DECLARATION OF INTERESTS

The authors declare no competing interests.

SUPPLEMENTAL INFORMATION

Supplemental information can be found online at https://doi.org/10.1016/j.joule.2024.09.013.

Received: January 29, 2024
Revised: April 2, 2024
Accepted: September 26, 2024
Published: November 8, 2024

REFERENCES

1. First Solar (2021). First solar series 6: advanced thin film solar technology. https://www.firstsolar.com/en-Emea/-/media/First-Solar/Technical-Documents/Series-6-Datasheets/Series-6-Datasheet.ashx.
2. First Solar (2022). First Solar Inc CDP Climate Change Questionnaire. J. Photon. Energy. https://www.firstsolar.com/-/media/First-Solar/Sustainability-Documents/2022-CDP-Climate-Change-Questionnaire_First-Solar.ashx.
3. Anctil, A., Beattie, M.N., Case, C., Chaudhary, A., Chrysler, B.D., Debije, M.G., Essig, S., Ferry, D.K., Ferry, V.E., Freitag, M., et al. (2023). Status report on emerging photovoltaics. J. Photonics Energy *13*, 42301.
4. NREL (2023). Research Cell Record Efficiency Chart. https://www.nrel.gov/pv/assets/pdfs/pv-efficiency-chart.201812171.pdf.
5. First Solar (2023). Series 7 TR1. https://www.firstsolar.com/-/media/First-Solar/Technical-Documents/Series-7/Series-7-TR1-High-Bin-Datasheet.ashx?la=en.
6. Green, M.A., Dunlop, E.D., Hohl-Ebinger, J., Yoshita, M., Kopidakis, N., and Hao, X. (2020). Solar Cell Efficiency Tables (version 56). Prog. Photovoltaics Res. Appl. *28*, 629–638.
7. Shockley, W., and Queisser, H.J. (1961). Detailed Balance Limit of Efficiency of p-n Junction Solar Cells. J. Appl. Phys. *32*, 510–519.

8. Ma, C., and Park, N.-G. (2020). A Realistic Methodology for 30% Efficient Perovskite Solar Cells. Chem *6*, 1254–1264.
9. Burst, J.M., Duenow, J.N., Albin, D.S., Colegrove, E., Reese, M.O., Aguiar, J.A., Jiang, C.S., Patel, M.K., Al-Jassim, M.M., Kuciauskas, D., et al. (2016). CdTe Solar Cells with Open-circuit Voltage Breaking the 1 V Barrier. Nat. Energy *1*, 16015.
10. Danielson, A., Reich, C., Pandey, R., Munshi, A., Onno, A., Weigand, W., Kuciauskas, D., Li, S., Bothwell, A., Guo, J., et al. (2023). Electro-optical Characterization of Arsenic-doped CdSeTe and CdTe Solar Cell Absorbers Doped in-situ during Close Space Sublimation. Sol. Energy Mater. Sol. Cells *251*, 112110.
11. Li, D.-B., Yao, C., Vijayaraghavan, S.N., Awni, R.A., Subedi, K.K., Ellingson, R.J., Li, L., Yan, Y., and Yan, F. (2021). Low temperature and Effective ex Situ Group V Doping for Efficient Polycrystalline CdSeTe Solar Cells. Nat. Energy *6*, 715–722.
12. Nagaoka, A., Nishioka, K., Yoshino, K., Katsube, R., Nose, Y., Masuda, T., and Scarpulla, M.A. (2020). Comparison of Sb, As, and P Doping in Cd-rich CdTe Single Crystals: Doping Properties, Persistent Photoconductivity, and Long-term Stability. Appl. Phys. Lett. *116*, 132102.
13. Krasikov, D., Guo, D., Demtsu, S., and Sankin, I. (2021). Comparative Study of As and Cu Doping Stability in CdSeTe Absorbers. Sol. Energy Mater. Sol. Cells *224*, 111012.
14. Metzger, W.K., Grover, S., Lu, D., Colegrove, E., Moseley, J., Perkins, C.L., Li, X., Mallick, R., Zhang, W., Malik, R., et al. (2019). Exceeding 20% Efficiency with in situ Group V Doping in Polycrystalline CdTe Solar Cells. Nat. Energy *4*, 837–845.
15. Colegrove, E., Yang, J.H., Harvey, S.P., Young, M.R., Burst, J.M., Duenow, J.N., Albin, D.S., Wei, S.H., and Metzger, W.K. (2018). Experimental and Theoretical Comparison of Sb, As, and P Diffusion Mechanisms and Doping in CdTe. J. Phys. D: Appl. Phys. *51*, 75102.
16. Danielson, A.H. (2022). Investigation of Group V Doping and Passivating Oxides to Reduce the Voltage Deficit in CdTe Solar Cells. For the Degree of Doctor of Philosophy (Colorado State University).
17. Jiang, C.S., Moseley, J., Xiao, C., Harvey, S., Farrell, S., Colegrove, E., Metzger, W.K., and Al-Jassim, M.M. (2020). Imaging Hole-density Inhomogeneity in Arsenic-doped CdTe Thin Films by Scanning Capacitance Microscopy. Sol. Energy Mater. Sol. Cells *209*, 110468.
18. Albin, D.S., Amarasinghe, M., Reese, M.O., Moseley, J., Moutinho, H., and Metzger, W.K. (2021). Colossal Grain Growth in Cd(Se,Te) Thin Films and Their Subsequent Use in CdTe Epitaxy by Close-spaced Sublimation. J. Phys. Energy *3*, 24003.
19. McCandless, B.E., Buchanan, W.A., Thompson, C.P., Sriramagiri, G., Lovelett, R.J., Duenow, J., Albin, D., Jensen, S., Colegrove, E., Moseley, J., et al. (2018). Overcoming Carrier Concentration Limits in Polycrystalline CdTe Thin Films with In Situ Doping. Sci. Rep. *8*, 14519.
20. Danielson, A., Munshi, A., Swanson, D., Drayton, J., Kartopu, G., Barth, K., Irvine, S., and Sampath, W. (2018). MOCVD Deposition of Group V Doped CdTe in Sublimated CdTe and CdSeTe Devices. In 2018 IEEE 7th World Conference on Photovoltaic Energy Conversion (WCPEC) (A Joint Conference of 45th IEEE PVSC, 28th PVSEC & 34th EU PVSEC), pp. 153–156.
21. Irvine, S.J.C., Oklobia, O., Jones, S., Lamb, D.A., Kartopu, G., Lu, D., and Xiong, G. (2023). Creating Metal Saturated growth in MOCVD for CdTe solar cells. J. Cryst. Growth *607*, 127124.
22. Kuciauskas, D., Nardone, M., Bothwell, A., Albin, D., Reich, C., Lee, C., and Colegrove, E. (2023). Why Increased CdSeTe Charge Carrier Lifetimes and Radiative Efficiencies did not Result in Voltage Boost for CdTe Solar Cells. Adv. Energy Mater. *13*, 2301784.
23. Mallick, R., Li, X., Reich, C., Shan, X., Zhang, W., Nagle, T., Bok, L., Bicakci, E., Rosenblatt, N., Modi, D., et al. (2023). Arsenic-Doped CdSeTe Solar Cells Achieve World Record 22.3% Efficiency. IEEE J. Photovoltaics, 510–515.
24. Oklobia, O., Jones, S., Kartopu, G., Lu, D., Miller, W., Mallick, R., Li, X., Xiong, G., Kornienko, V., Abbas, A., et al. (2022). Impact of In-Situ Cd Saturation MOCVD Grown CdTe Solar Cells on As Doping and V_{OC}. IEEE J. Photovoltaics *12*, 1296–1302.
25. Xiong, G. (2021). Doping Method with Potential. Nat. Energy *6*, 694–695.
26. Tari, S., Aqariden, F., Chang, Y., Ciani, A., Grein, C., Li, J., and Kioussis, N. (2014). Structural and Electronic Properties of Gold Contacts on CdZnTe with Different Surface Finishes for Radiation Detector Applications. J. Electron. Mater. *43*, 2978–2983.
27. Li, D.-B., Bista, S.S., Awni, R.A., Neupane, S., Abudulimu, A., Wang, X., Subedi, K.K., Jamarkattel, M.K., Phillips, A.B., Heben, M.J., et al. (2022). 20%-efficient Polycrystalline Cd(Se,Te) Thin-film Solar Cells with Compositional Gradient near the Front Junction. Nat. Commun. *13*, 7849.
28. Li, D.-B., Neupane, S., Bista, S.S., Xiao, C., Abudulimu, A., Jamarkattel, M.K., Phillips, A.B., Heben, M.J., Poplawsky, J.D., Cullen, D.A., et al. (2023). Oxygen Management to Avoid Photo-Inactive Cd(S,Se) for Efficient Cd(Se,Te) Solar Cells. ACS Energy Lett. *8*, 1529–1534.
29. Bista, S.S., Li, D.-B., Awni, R.A., Song, Z., Subedi, K.K., Shrestha, N., Rijal, S., Neupane, S., Grice, C.R., Phillips, A.B., et al. (2021). Effects of a Cu Precursor on the Performance of Efficient CdTe Solar Cells. ACS Appl. Mater. Interfaces *13*, 38432–38440.
30. Li, D.-B., Bista, S.S., Song, Z., Alfadhili, F.K., Awni, R.A., Shrestha, N., Rhiannon, D., Phillips, A.B., Heben, M.J., Ellingson, R.J., et al. (2020). CuSCN as the Back Contact for Efficient ZMO/CdTe Solar. Cells Mater. (Basel) *13*, 1991.
31. Jiang, C.-S., Albin, D., Nardone, M., Howard, K.J., Danielson, A., Munshi, A., Shimpi, T., Xiao, C., Moutinho, H.R., Al-Jassim, M.M., et al. (2022). Electrical Potential Investigation of Reversible Metastability and Irreversible Degradation of CdTe Solar Cells. Sol. Energy Mater. Sol. Cells *238*, 111610.
32. Moutinho, H.R., Dhere, R.G., Jiang, C.-S., Yan, Y., Albin, D.S., and Al-Jassim, M.M. (2010). Investigation of Potential and Electric Field Profiles in Cross Sections of CdTe/CdS Solar Cells Using Scanning Kelvin Probe Microscopy. J. Appl. Phys. *108*, 74503.
33. Kresse, G., and Furthmüller, J. (1996). Efficiency of Ab-initio Total Energy Calculations for Metals and Semiconductors Using a Plane-Wave Basis Set. Computational Materials Science *6*, 15–50.
34. Kresse, G., and Furthmüller, J. (1996). Efficient Iterative Schemes for Ab Initio Total-energy Calculations Using a Plane-wave Basis Set. Phys. Rev. B Condens. Matter *54*, 11169–11186.
35. Blöchl, P.E. (1994). Projector Augmented-wave Method. Phys. Rev. B Condens. Matter *50*, 17953–17979.
36. Heyd, J., Scuseria, G.E., and Ernzerhof, M. (2003). Hybrid Functionals Based on a Screened Coulomb Potential. J. Chem. Phys. *118*, 8207–8215.
37. Monkhorst, H.J., and Pack, J.D. (1976). Special Points for Brillouin-Zone Integrations. Phys. Rev. B *13*, 5188–5192.